ACS Photonics

Article

pubs.acs.org/journal/apchd5

From Thermo- to Plasma-Mediated Ultrafast Laser-Induced Plasmonic Nanobubbles

Rémi Lachaine, Étienne Boulais,† and Michel Meunier*

Laser Processing and Plasmonics Laboratory, Engineering Physics Department, École Polytechnique de Montréal, Montréal, Québec H3C 3A7, Canada

Supporting Information

ABSTRACT: The laser-induced generation of vapor bubbles around gold nanoparticles (AuNPs) is a promising diagnostic and therapeutic avenue for various pathologies. The physical mechanism that leads to their formation strongly depends on the time regime of the irradiation. While the plasmonic nanobubbles induced by nanosecond and picosecond laser pulses are known to be triggered by the energy that is absorbed in the nanoparticles and diffused in the medium (thermo-mediated cavitation), we show that a different plasma-mediated mechanism occurs in the case of femtosecond pulses. In this paper, we present experimental evidence that the dimensions of laser-induced bubbles depend on the polarization of the incident laser pulse when the pulse duration is reduced below ∼1 ps. This result cannot be explained by the standard thermo-mediated cavitation process and, thus, reveals the onset of a new mechanism in the ultrafast regime. We further show that the discrepancy between the dimensions of bubbles generated from linearly and circularly polarized laser pulses can be explained using a simple model, revealing the polarization cavitation dependence as a clear signature of the plasma mechanism. This paper presents in detail the transition between both cavitation regimes and provides insight into the precise control of the cavitation dynamics at the nanoscale.

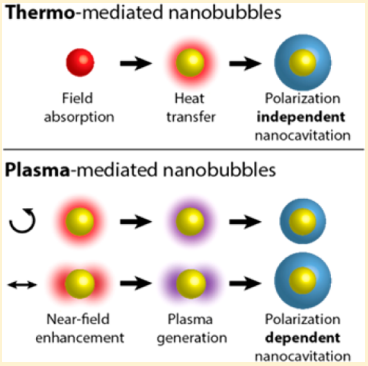

KEYWORDS: *nanoplasma, plasmonics, nanoparticles, bubbles, nanocavitation*

The generation of plasmonic nanobubbles has drawn considerable attention in the past few years. Their use in cell nanosurgery applications[1] such as photothermal therapy,[2−7] cell membrane optoporation,[8−10] and drug delivery[11−15] makes them a promising and valuable tool in the field of biomedical applications. In particular, significant progress has been made toward controlling and optimizing the plasmonic properties of nanomaterials,[16] enabling various applications including steam generation[17] and cancer treatment.[18,19] To date, choosing the optimal laser source and plasmonic nanostructure to induce nanocavitation in the most effective and safest way remains a challenge. Irradiating gold nanoparticles (AuNPs) with nanosecond laser pulses, at a wavelength that matches their plasmon resonance, is an approach commonly used to generate nanobubbles in both water and biological mediums.[1−9,11,12,20] In this method (Figure 1a), photons from the laser pulse excite a plasmon (a quantified oscillation of the electrons) in the AuNPs. This resonant phenomenon results in an exceptionally large optical energy transfer to the AuNPs. The surrounding liquid is then rapidly heated from a conductive process at the interface. Within ∼0.1−1 ns, a combination of explosive boiling and phase explosion transforms the liquid into a thermo-mediated vapor bubble. While efficient, this method relies on the extreme heating of the AuNP and can provoke its fragmentation and degradation, thus leading to important issues concerning multipulses and scanning procedures. In addition, in the context of biological applications, serious toxicity concerns are raised by the presence of small gold fragments that could possibly intercalate in DNA of living cells.[21]

Using ultrashort laser pulses for the processing of material is usually associated with enhanced precision and reduced collateral damage, due to limited impact from thermal diffusion and very fast phase transformation.[22] Interested in exploiting those expected benefits, Koitadis et al. have studied the possibility of generating nanobubbles by irradiating AuNPs with femtosecond laser pulses, using a wavelength nearly tuned to their plasmon resonance.[23,24] While their results revealed a much lower fluence threshold to initiate bubble formation than for nanosecond pulses, cavitation still relies on the extreme heating of the AuNPs, which are indeed found to be heavily damaged during the procedure, in agreement with another work from Yelin et al.[25]

Our group has recently proposed a novel ultrashort laser based nanocavitation approach that uses an off-resonance wavelength to form nanobubbles around AuNPs without inducing any deformation or fragmentation.[10,26] Using a wavelength slightly detuned from the plasmon resonance, only a small fraction of the deposited energy is absorbed in the AuNPs, explaining the conservation of their structural integrity. Following the conclusion of our previous work,[26,27] the main mechanism leading to nanocavitation in that case is hypothesized to result from the creation of an energetic

Received: August 30, 2013
Published: March 31, 2014

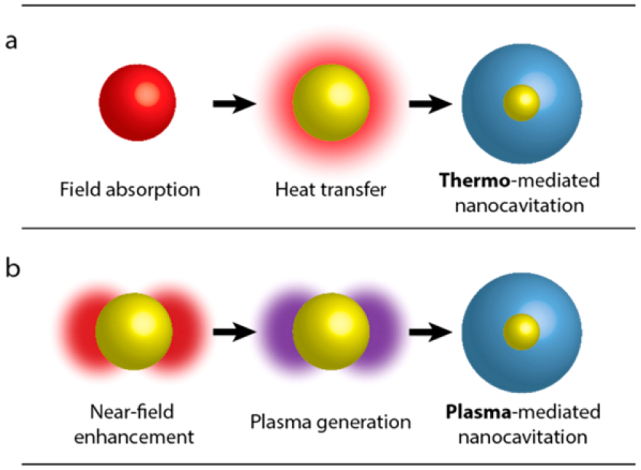

Figure 1. Schematic comparison of thermo-mediated and plasma-mediated nanocavitation mechanisms. (a) Thermo-mediated nanocavitation. Electric field absorption in the particle leads to the extreme heating of this particle. This heat then transfers to the surrounding water and in turn leads to thermo-mediated nanocavitation. (b) Plasma-mediated nanocavitation. Near-field enhancement around the particle leads to plasma generation in the water through multiphotonic ionization. This plasma then relaxes and transfers its energy to the water, which in turn leads to plasma-mediated nanocavitation.

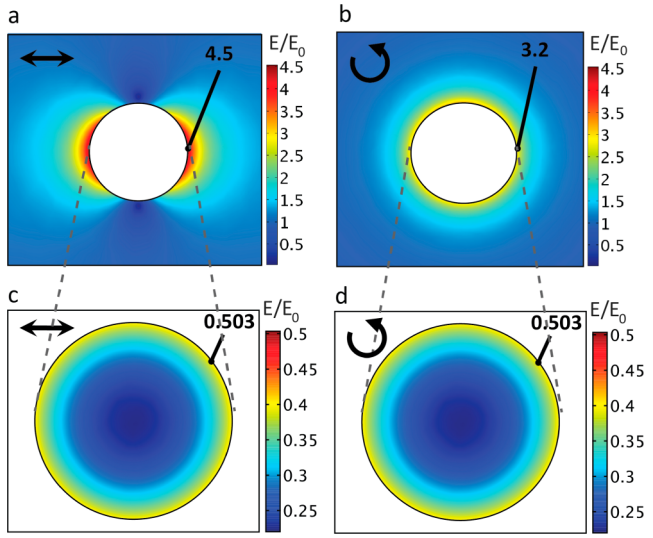

Figure 2. Polarization dependence of the electric field enhancement around a 100 nm gold nanoparticle in water. In both cases, laser propagation is perpendicular to the figure plane. (a) Enhancement of a linearly polarized field is distributed at the poles of the particle, and the maximum enhancement is ∼4.5. (b) Enhancement of a circularly polarized field is distributed all around the nanoparticle with a maximum of ∼3.2. (c) Absorbed field distribution inside the NP for linear polarization. (d) Absorbed field distribution inside the NP for circular polarization.

nanoplasma around the AuNP from the nonlinear photoionization of the water molecules directly in the plasmon-enhanced near-field. Relaxation of this plasma then transfers energy to the water in a few picoseconds, thus inducing a plasma-mediated nanocavitation. This mechanism is in agreement with recent work from Halas et al., who also attributed to the generation of hot electrons (plasma) the plasmon-induced dissociation of H_2 molecules around AuNPs.[28]

These two cavitation mechanisms, and in particular the transition from the thermo-mediated mechanism to the plasma-mediated mechanism, have never been directly observed from a simple experiment. In order to deepen our understanding of the cavitation mechanism, it would be desirable to be able to characterize which type of cavitation is dominant for a given set of experimental parameters. In particular, it would be interesting to observe the transition from a thermo-mediated to a plasma-mediated cavitation as the pulse duration of the incident laser is decreased. In the following, we demonstrate that this transition can be easily detected using the dependence on polarization of the size of the bubbles produced around the AuNPs.

To understand how polarization affects cavitation, we have numerically investigated the polarization dependence of the field enhancement around a 100 nm AuNP in water. Figure 2 compares the simulated field enhancement distribution for an incident 800 nm laser with (a) linear polarization and (b) circular polarization. The maximum enhancement of ∼4.5 calculated in the case of a linear polarization drops to only ∼3.2 in the case of a circular polarization. Unsurprisingly, the maximum enhancement for the circular polarization corresponds to $1/\sqrt{2}$ times the one induced by the linear polarization, which was expected from spherical symmetry of the NP. In opposition, the field distribution inside the NP is almost the same for both polarizations. Indeed, as shown on Figure 2c and d, the field distribution inside the NP has a radial symmetry for the linear polarization and, therefore, remains unaffected by the switch to a circular polarization.

If the near-field intensity is sufficient, nonlinear photoionization of the water molecules can occur, leading to the generation of a nanoscale plasma. If this occurs, the different field distribution implies that the energy deposition should be polarization dependent. In a plasma-mediated cavitation mechanism, it is the energy transfer from this plasma to the water molecule that is at the origin of the bubble, not the energy transfer coming from the AuNP heating. In a first approximation, it is reasonable to assume that the size of the bubble is proportional to the deposited energy.[29] Because the field enhancement depends on the polarization, a plasma-mediated mechanism should also imply polarization-dependent bubble sizes. As schematically summarized in Figure 3, in the case of plasma-mediated nanocavitation, larger field enhancement leads to more energetic plasma production and in turn leads to larger nanobubbles.

In opposition, the very similar field distribution inside the nanoparticle implies that energy deposited inside the AuNP is independent of polarization. The size of the thermo-mediated bubble should in consequence not be influenced by the incident polarization. Hence, the polarization dependence of the size of the plasmonic nanobubbles can be interpreted as a clear signature of a plasma-mediated cavitation mechanism, while polarization independence indicates cavitation that is mostly thermo-mediated.

These theoretical results suggest that one could experimentally measure and compare the sizes of the nanobubbles produced with a linear and a circular polarization to determine whether they have been produced from a thermo-mediated or a plasma-mediated mechanism. Polarization dependence of the nanobubble size can thus be used as a convenient tool to distinguish the dominant cavitation mechanism.

On the basis of this principle, we have investigated the mechanisms responsible for cavitation around AuNPs with a diameter of 100 nm in a water suspension irradiated with 180

dx.doi.org/10.1021/ph400018s | ACS Photonics 2014, 1, 331−336

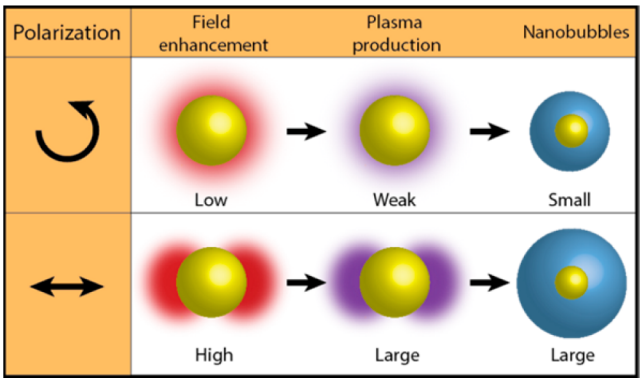

Figure 3. Schematic representation of the polarization dependence of the plasma-mediated nanocavitation. Linearly polarized pulses induce higher field enhancement (red) and higher plasma production (purple) and leads to larger nanobubbles (blue) than pulses with a circular polarization.

mJ/cm^2 single laser pulses, at a wavelength of 800 nm and with a pulse duration ranging from 45 fs to 8.8 ps using linear and circular polarization. Figure 4 compares the probe laser time-resolved signal following the irradiation of the AuNPs with a linear and circular polarization for (a) 45 fs and (b) 1 ps pump laser pulses at the exact same fluence (180 mJ/cm^2). Figure 4a clearly demonstrates a significant difference between both polarizations for femtosecond pulses. The maximal amplitude is indeed much larger for linear polarization, suggesting that the nanobubbles produced in that case are larger than those created from a circular polarization. In addition, the time position corresponding to the maximal amplitude is also larger, which indicates a larger bubble lifetime. Considering the Rayleigh–Plesset relation,[30,31] which relates the bubble lifetime to the maximal diameter ($\tau \approx 0.092 d_{max}$), both observations agree with the nanobubbles being larger when produced with a linearly polarized beam. From the discussion presented above, it can thus be concluded that, for 45 fs pulses, the nanocavitation mechanism is mostly plasma-mediated.

In contrast, for longer pulses (1 ps), Figure 4b shows that the signals associated with both polarizations are very similar in terms of both amplitude and lifetime. This result suggests that the induced bubbles are very comparable in size and are thus polarization independent. As discussed above, this is consistent with a cavitation that is mostly thermo-mediated. Note that the signal amplitudes in Figure 4b are smaller than in Figure 4a, indicating that femtosecond pulses generate larger bubbles than picosecond pulses. This observation has already been discussed in a previous publication[32] and is consistent with the additional nonlinear energy deposition characteristic of the plasma-mediated cavitation process.

The same experiment has been repeated for various pulse durations between 45 fs and 8.8 ps, for both circular and linear polarization of the pump laser pulse, at a fluence of 180 mJ/cm^2 (Figure 5a). Using the coated Mie theory, the NP concentration, and the beam's characteristic, it is further possible to approximately deduce the maximal diameters of the bubble needed to explain the scattering losses suffered by the probe laser beam. More details on this procedure can be found in previous publications[26,32] and in the Supporting Information Note 2. The ratio of the deduced average diameter of the bubbles at their maximal extension produced with a linear polarization over those generated with a circular polarization is shown by the blue curve in Figure 5b. Note that the nonlinear relation between scattering losses and bubble diameters[32] affects the ratio profile, thus explaining why some signal amplitudes' ratios are higher than their corresponding deduced bubble diameters' ratio. Both results show that very similar bubbles are produced by both polarizations for long pulses. Then, the bubbles produced by linearly polarized pulses get progressively bigger than those induced by circularly polarized pulses as the pulse duration is reduced to the femtosecond regime. These results are consistent with a transition from a longer pulse thermo-mediated cavitation mechanism to the femtosecond plasma-mediated cavitation mechanism, with a pulse duration threshold of ~1 ps separating the two regimes.

We then used a partial differential equation based numerical model to calculate the theoretical linear over circular bubble deposited energy in the water to compare it with the experimental observation, in order to assess the plausibility of the thermo- and plasma-mediated cavitation mechanisms and of the pulse duration that separates the two regimes. The simulated ratios are shown by the green and red curves in Figure 5. The green curve shows the ratio assuming that the bubble maximal volume is directly proportional to the deposited energy. This proportionality is intuitive and has been reported elsewhere.[29] However, a small but significant discrepancy with the experimental data remains. The red curve

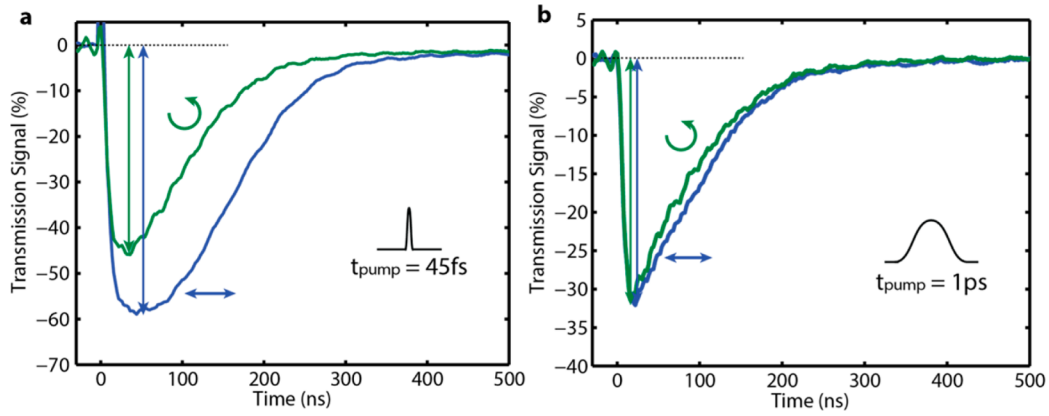

Figure 4. Polarization dependence of the nanobubbles scattering signal. Nanobubbles have been generated with an average fluence of 180 mJ/cm^2 around 100 nm AuNPs in water. (a) Nanobubbles generated with a 45 fs pulse duration. A large difference between the signals can be observed. (b) Nanobubbles generated with a 1 ps pulse duration. No significant difference between the signals can be observed.

dx.doi.org/10.1021/ph400018s | ACS Photonics 2014, 1, 331–336

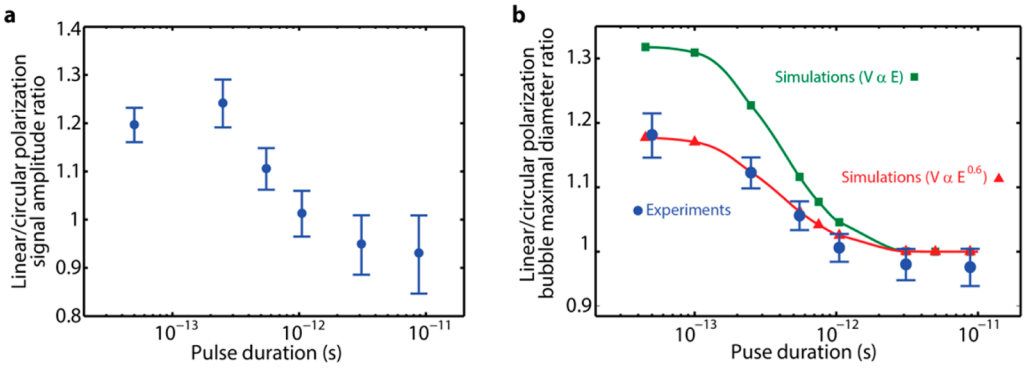

Figure 5. Ratios of the bubbles generated with linear polarization over bubbles generated with circular polarization for different laser pulse durations. (a) Experimental ratio of the signal amplitudes coming from bubbles produced with a linear polarization over the ones produced with a circular polarization as a function of pulse duration for an average fluence of 180 mJ/cm^2. Error bars come from the uncertainty in the signal amplitude determination caused by the remaining noise in the signal after averaging. Standard deviation of this noise has been considered. (b) Ratio of the maximum diameter of bubbles produced with a linear polarization over the ones produced with a circular polarization for the same average fluence. Experimental maximum diameter ratios deduced from the signal amplitudes are shown by the blue dots. Green squares show the simulation results assuming that the bubble volume (V) is proportional to the deposited energy (E), whereas the red triangles show the same simulation when $V \propto E^{0.6}$.

shows a much better fit (R^2= 0.96) when a $V = E^{0.6}$ relation between the deposited energy and the bubble volume is used, rather than a direct proportionality. This lower than unity exponent might be explained by the energetic losses due to surface tension effects and pressure wave generation that become increasingly important respectively at the nanoscale and in the ultrafast regime. The fact that the bubble should grow from an initially asymmetric shape, especially for the linear polarization, could also contribute to this lower than unity exponent. In addition, the size distribution of AuNPs as well as some imperfection in the beam polarization might also contribute to the experimental discrepancy with the theoretical results. Also, the diameter ratios deduced from the experimental results assume that the focal volume inside which bubbles are created is the same for both polarizations (see Supporting Information Note 2), which is probably not the case for the plasma-mediated mechanism. However, while this may affect the deduced experimental diameter ratio, it does not contradict the conclusion, as the plasma-mediated mechanism must be invoked to justify this probable change in focal volume. It is thus possible that this fitted exponent reflects only the nonideal conditions of the experiments. In any case, both simulated results clearly show a 1 ps threshold between the polarization-independent thermo-mediated cavitation and the polarization-dependent plasma-mediated cavitation, in almost perfect agreement with the experimental result.

In summary, we were able to reveal the existence of two regimes of laser-induced plasmon-enhanced nanocavitation. Using an all-optical method, we showed a clear transition from polarization-independent to polarization-dependent cavitation regime when the pulse duration is reduced below ~1 ps, supported by our simulation results. For long pulses, the cavitation is due to the laser energy absorption in the AuNPs, followed by its conductive transfer at the water interface. Since the electric field distribution in the AuNP is polarization independent, our results indicate that this thermo-mediated cavitation mechanism is consistent with a polarization-independent cavitation. However, the polarization dependence shown for femtosecond pulses indicates the appearance of another regime. For those shorter pulses, our results indicate that cavitation is rather plasma-mediated, resulting from the nonlinear interaction of the enhanced laser field with the water molecules directly in the near-field, creating a localized photoexcited plasma that yields the bubble. Our numerical modeling indicates that the ratio experimentally observed between the maximal diameters of bubbles produced from a linearly and circularly polarized laser is consistent with this plasma-mediated mechanism. This work significantly strengthens the actual understanding of the physical mechanisms occurring in plasmon-enhanced laser nanocavitation. This new understanding should contribute to the development of novel efficient nanobubble production methods, in particular in the field of cell nanosurgery, where fragmentation of the AuNPs and collateral damage to the cells remain a critical issue.

EXPERIMENTAL METHODS

A rotating $\lambda/4$ waveplate was used to change the polarization from linear to circular. The method used to characterize the size of the nanobbubles consists in a low-intensity continuous wave HeNe probe laser aligned along with the femtosecond pump laser. Both beams are focused into a 1 × 1 cm^2 quartz cuvette containing 1 mL of the AuNP solution. The scattering losses of the probe laser due to the presence of nanobubbles are filtered out using a spatial filter, and the size and lifetimes of the nanobubbles induced by the pump laser are characterized from the probe laser time-resolved amplitude collected with a Si 1 GHz photoreceiver. The interested reader is referred to other works for further details on the method.[26,32,33]

The model includes the description of both the thermo-mediated and plasma-mediated cavitation mechanism and is based on previous publications.[26,33] The Helmholtz equation is used to calculate the field distribution around and inside the nanoparticle. In addition to absorption in the AuNP, the electric field in the near-field may also create a low-density plasma, by a combination of photoionization and collision ionization, the density and temperature of which are calculated using the standard transport equation. The plasma around the AuNP also significantly modifies the optical properties of the medium, which is taken into consideration by introducing a time-dependent dielectric function. The mathematical model is solved using a time-dependent finite-element method in tridimensional space. This model allows calculating the total energy being deposited in the water surrounding the AuNP

dx.doi.org/10.1021/ph400018s | ACS Photonics 2014, 1, 331−336

during the laser pulse. Details on the modeling can be found in the Supporting Information Note 1.

The ratio between the energy deposited by a linearly and a circularly polarized beam can thus be evaluated. From the energy ratio, a diameter ratio is deduced, assuming different proportionality between the volume of the bubble produced (V) and the deposited energy (E). In a first approximation, we hypothesize that the maximal bubble volume depends only on the energy deposited during the laser pulse and is thus independent of the specific subsequent hydro- and thermodynamic evolution of the system. A direct proportionality between the volume and deposited energy ($V \sim E$) is intuitive and has been reported by Putsovalov et al.[29] Experimental measurements from Siems et al.[34] rather reported $V \sim E^{1.35}$ for AuNPs irradiated with femtosecond laser pulses tuned to their plasmon resonance. We thus hypothesize that a relation $V \sim E^{\alpha}$ can be used to characterize the bubble dimensions, with an exponent α that will be adjusted to our experimental data. The Gaussian energy distribution of both the pump and probe laser beams has also been taken into consideration when evaluating the theoretical energy ratio. The reader is referred to the above-cited literature and to the Supporting Information Note 3 for addition details on the ratio determination.

■ ASSOCIATED CONTENT

Supporting Information

Details on the modeling. This material is available free of charge via the Internet at http://pubs.acs.org.

■ AUTHOR INFORMATION

Corresponding Author

*E-mail: michel.meunier@polymtl.ca.

Present Address

[†]Department of Biological Engineering, Massachusetts Institute of Technology, 77 Massachusetts Avenue, Cambridge, Massachusetts 02139, United States.

Notes

The authors declare no competing financial interest.

■ ACKNOWLEDGMENTS

The authors would like to thank the Natural Science and Engineering Research Council (NSERC) and Le Fond Québecois de la Recherche sur la Nature et les Technologies (FQRNT) for financial support, Ali Hatef, Alexandra Thibeault-Eybalin, Christos Boutopoulos, David Rioux, Éric Bergeron, and Weimeng Ding for their valuable discussions, and Yves Drolet for his technical support.

■ REFERENCES

(1) Boulais, E.; Lachaine, R.; Hatef, A.; Meunier, M. Plasmonics for pulsed-laser cell nanosurgery: Fundamentals and applications. *J. Photochem. Photobiol., C* **2013**, *17*, 26−49.

(2) Pitsillides, C. M.; Joe, E. K.; Wei, X.; Anderson, R.; Lin, C. P. Selective cell targeting with light-absorbing microparticles and nanoparticles. *Biophys. J.* **2003**, *84*, 4023−4032.

(3) Kitz, M.; Preisser, S.; Wetterwald, a; Jaeger, M.; Thalmann, G. N.; Frenz, M. Vapor bubble generation around gold nano-particles and its application to damaging of cells. *Biomed. Opt. Express* **2011**, *2*, 291−304.

(4) Zharov, V. P.; Galitovsky, V.; Viegas, M. Photothermal detection of local thermal effects during selective nanophotothermolysis. *Appl. Phys. Lett.* **2003**, *83*, 4897−4899.

(5) Zharov, V. P.; Mercer, K. E.; Galitovskaya, E. N.; Smeltzer, M. S. Photothermal nanotherapeutics and nanodiagnostics for selective killing of bacteria targeted with gold nanoparticles. *Biophys. J.* **2006**, *90*, 619−627.

(6) Huang, X.; Kang, B.; Qian, W.; Mackey, M. A.; Chen, P. C.; Oyelere, A. K.; El-Sayed, I. H.; El-Sayed, M. A. Comparative study of photothermolysis of cancer cells with nuclear-targeted or cytoplasm-targeted gold nanospheres: continuous wave or pulsed lasers. *J. Biomed. Opt.* **2010**, *15*, 058002.

(7) Wagner, D. S.; Delk, N. A.; Lukianova-Hleb, E. Y.; Hafner, J. H.; Farach-Carson, M. C.; Lapotko, D. O. The in vivo performance of plasmonic nanobubbles as cell theranostic agents in zebrafish hosting prostate cancer xenografts. *Biomaterials* **2010**, *31*, 7567−7574.

(8) Yao, C.; Rahmanzadeh, R.; Endl, E.; Zhang, Z.; Gerdes, J.; Huttmann, G. Elevation of plasma membrane permeability by laser irradiation of selectively bound nanoparticles. *J. Biomed. Opt.* **2005**, *10*, 64012−64018.

(9) Lukianova-Hleb, E. Y.; Samaniego, A. P.; Wen, J.; Metelitsa, L. S.; Chang, C.-C.; Lapotko, D. O. Selective gene transfection of individual cells in vitro with plasmonic nanobubbles. *J. Controlled Release* **2011**, *152*, 286−293.

(10) Baumgart, J.; Humbert, L.; Boulais, É.; Lachaine, R.; Lebrun, J. J.; Meunier, M. Off-resonance plasmonic enhanced femtosecond laser optoporation and transfection of cancer cells. *Biomaterials* **2011**, *33*, 2345−2350.

(11) Anderson, L. J. E.; Hansen, E.; Lukianova-Hleb, E. Y.; Hafner, J. H.; Lapotko, D. O. Optically guided controlled release from liposomes with tunable plasmonic nanobubbles. *J. Controlled Release* **2010**, *144*, 151−158.

(12) Lukianova-Hleb, E. Y.; Belyanin, A.; Kashinath, S.; Wu, X.; Lapotko, D. O. Plasmonic nanobubble-enhanced endosomal escape processes for selective and guided intracellular delivery of chemotherapy to drug-resistant cancer cells. *Biomaterials* **2012**, *33*, 1821−1826.

(13) Ibrahimkutty, S.; Kim, J.; Cammarata, M.; Ewald, F.; Choi, J.; Ihee, H.; Plech, A. Ultrafast structural dynamics of the photocleavage of protein hybrid nanoparticles. *ACS Nano* **2011**, *5*, 3788−3794.

(14) Huschka, R.; Barhoumi, A.; Liu, Q.; Roth, J. A.; Ji, L.; Halas, N. J. Gene silencing by gold nanoshell-mediated delivery and laser-triggered release of antisense oligonucleotide and siRNA. *ACS Nano* **2012**, *6*, 7681−7691.

(15) Bisker, G.; Yeheskely-Hayon, D.; Minai, L.; Yelin, D. Controlled release of Rituximab from gold nanoparticles for phototherapy of malignant cells. *J. Controlled Release* **2012**, *162*, 303.

(16) Halas, N. J.; Lal, S.; Link, S.; Chang, W.-S.; Natelson, D.; Hafner, J. H.; Nordlander, P. A plethora of plasmonics from the Laboratory for Nanophotonics at Rice University. *Adv. Mater.* **2012**, *24*, 4774.

(17) Fang, Z.; Zhen, Y.-R.; Neumann, O.; Polman, A.; de Abajo, F. J. G.; Nordlander, P.; Halas, N. J. Evolution of light-induced vapor generation at a liquid-immersed metallic nanoparticle. *Nano Lett.* **2013**, *13*, 1736−1742.

(18) Lukianova-Hleb, E. Y.; Ren, X.; Zasadzinski, J. A.; Wu, X.; Lapotko, D. Plasmonic nanobubbles enhance efficacy and selectivity of chemotherapy against drug-resistant cancer cells. *Adv. Mater.* **2012**, *24*, 3831−3837.

(19) Bardhan, R.; Lal, S.; Joshi, A.; Halas, N. J. Theranostic nanoshells: from probe design to imaging and treatment of cancer. *Acc. Chem. Res.* **2011**, *44*, 936−946.

(20) Lukianova-Hleb, E. Y.; Hu, Y.; Latterini, L.; Tarpani, L.; Lee, S.; Drezek, R.; Hafner, J. H.; Lapotko, D. O. Plasmonic nanobubbles as transient vapor nanobubbles generated around plasmonic nanoparticles. *ACS Nano* **2010**, *4*, 2109−2123.

(21) Schaeublin, N. M.; Braydich-Stolle, L. K.; Schrand, A. M.; Miller, J. M.; Hutchison, J.; Schlager, J. J.; Hussain, S. M. Surface charge of gold nanoparticles mediates mechanism of toxicity. *Nanoscale* **2011**, *3*, 410−420.

(22) Chichkov, B. N.; Momma, C.; Nolte, S.; Von Alvensleben, F.; Tünnermann, A. Femtosecond, picosecond and nanosecond laser ablation of solids. *Appl. Phys. A: Mater. Sci. Process.* **1996**, *63*, 109−115.
(23) Kotaidis, V.; Plech, A. Cavitation dynamics on the nanoscale. *Appl. Phys. Lett.* **2005**, *87*, 213101−213102.
(24) Plech, A.; Kotaidis, V.; Lorenc, M.; Boneberg, J. Femtosecond laser near-field ablation from gold nanoparticles. *Nat. Phys.* **2006**, *2*, 44−47.
(25) Warshavski, O.; Minai, L.; Bisker, G.; Yelin, D. Effect of single femtosecond pulses on gold nanoparticles. *J. Phys. Chem. C* **2011**, *115*, 3910.
(26) Boulais, E.; Lachaine, R.; Meunier, M. Plasma mediated off-resonance plasmonic enhanced ultrafast laser-induced nanocavitation. *Nano Lett.* **2012**, *12*, 4763−4769.
(27) Ostrikov, K.; Neyts, E. C.; Meyyappan, M. Plasma nanoscience: from nano-solids in plasmas to nano-plasmas in solids. *Adv. Phys.* **2013**, *62*, 113−224.
(28) Mukherjee, S.; Libisch, F.; Large, N.; Neumann, O.; Brown, L. V.; Cheng, J.; Lassiter, J. B.; Carter, E. A.; Nordlander, P.; Halas, N. J. Hot electrons do the impossible: plasmon-induced dissociation of H2 on Au. *Nano Lett.* **2013**, *13*, 240−247.
(29) Pustovalov, V. K.; Smetannikov, A. S.; Zharov, V. P. Photothermal and accompanied phenomena of selective nano-photothermolysis with gold nanoparticles and laser pulses. *Laser Phys. Lett.* **2008**, *5*, 775−792.
(30) Neumann, J.; Brinkmann, R. Self-limited growth of laser-induced vapor bubbles around single microabsorbers. *Appl. Phys. Lett.* **2008**, *93*, 033901−033901−3.
(31) Plesset, M. S.; Prosperetti, A. Bubble dynamics and cavitation. *Annu. Rev. Fluid Mech.* **1977**, *9*, 145−185.
(32) Lachaine, R.; Boulais, E.; Bourbeau, E.; Meunier, M. Effect of pulse duration on plasmonic enhanced ultrafast laser-induced bubble generation in water. *Appl. Phys. A: Mater. Sci. Process.* **2012**, *112*, 119−122.
(33) Boulais, E.; Lachaine, R.; Meunier, M. Plasma-mediated nanocavitation and photothermal effects in ultrafast laser irradiation of gold nanorods in water. *J. Phys. Chem. C* **2013**, *117*, 9386−9396.
(34) Siems, A.; Weber, S.; Boneberg, J.; Plech, A. Thermodynamics of nanosecond nanobubble formation at laser-excited metal nanoparticles. *New J. Phys.* **2011**, *13*, 043018-1−043012-22.